

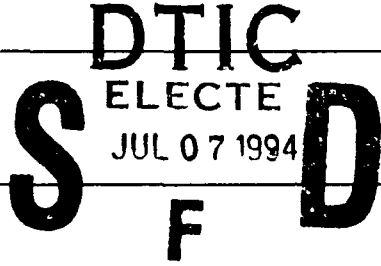

AD-A281 182



ION PAGE

Form Approved
OMB No. 0704-0188

Public reporting burden for this collection of information is estimated to average 1 hour per response, including the time for reviewing instructions, searching existing data sources, gathering and maintaining the data needed, reviewing existing materials, collecting, reviewing, and completing the review of information, including the time for reviewing instructions, searching existing data sources, gathering and maintaining the data needed, reviewing existing materials, collecting, reviewing, and completing the review of information, including comments regarding this burden estimate or any other aspect of this collection of information, including suggestions for reducing the burden, and to the Office of Management and Budget, Paperwork Reduction Project (0704-0188), Washington, DC 20503.

1 AGENCY USE ONLY (Leave blank)	2 REPORT DATE June 1994	3 REPORT TYPE AND DATES COVERED Professional Paper
4 TITLE AND SUBTITLE ACOUSTIC COMPUTATIONS FOR A LOW MACH NUMBER HEATED CYLINDER	5 FUNDING NUMBERS In-house funding	
6 AUTHOR(S) T. S. Mautner	7 PERFORMING ORGANIZATION NAME(S) AND ADDRESS(ES) Naval Command, Control and Ocean Surveillance Center (NCCOSC) RDT&E Division San Diego, CA 92152-5001	
8 PERFORMING ORGANIZATION REPORT NUMBER	9 SPONSORING/MONITORING AGENCY NAME(S) AND ADDRESS(ES) Naval Command, Control and Ocean Surveillance Center (NCCOSC) RDT&E Division San Diego, CA 92152-5001	
10 SPONSORING/MONITORING AGENCY REPORT NUMBER	11 SUPPLEMENTARY NOTES	
		
12a DISTRIBUTION/AVAILABILITY STATEMENT	11095 94-20614 	
Approved for public release; distribution is unlimited.		

13 ABSTRACT (Maximum 200 words)

This paper describes the sound generated by uniform flow over a heated cylinder, calculated for a range of Reynolds and Grashof numbers. The time-dependent, incompressible flow field is computed using a vorticity-stream function method containing the Boussinesq approximation. Using the computed incompressible flow field, the radiated sound is computed using a low frequency Green's function technique. Snapshots of the vorticity and temperature fields and time histories of the radiated sound pressure are presented and compared with existing results.

DTIC QUALITY CENTER

94 7 6 064

Published in *Proceedings, 32nd Aerospace Sciences Meeting and Exhibit*, pp. 1-13, January 1994.

14 SUBJECT TERMS Computational Acoustics (CA) heated cylinder		15 NUMBER OF PAGES
		16 PRICE CODE
17 SECURITY CLASSIFICATION OF REPORT UNCLASSIFIED	18 SECURITY CLASSIFICATION OF THIS PAGE UNCLASSIFIED	19 SECURITY CLASSIFICATION OF ABSTRACT UNCLASSIFIED
20 LIMITATION OF ABSTRACT SAME AS REPORT		

**Best
Available
Copy**

UNCLASSIFIED

21a NAME OF RESPONSIBLE INDIVIDUAL T. S. Mautner	21b TELEPHONE (include Area Code) (619) 553-1621	21c OFFICE SYMBOL Code 574
---	---	-------------------------------

Accession For	
NTIS CRA&I	✓
DTIC TAB	
Unannounced	
Justification	
By	
Distribution /	
Availability	
Dist	Avail Spec
A-1	20



AIAA 94-0360

**ACOUSTIC COMPUTATIONS FOR A LOW MACH
NUMBER HEATED CYLINDER WAKE FLOW**

T. S. Mautner

Naval Command, Control & Ocean

Surveillance Center RDTE Division

San Diego, CA 92152

**32nd Aerospace Sciences
Meeting & Exhibit
January 10-13, 1994 / Reno, NV**

ACOUSTIC COMPUTATIONS FOR A LOW MACH NUMBER HEATED CYLINDER WAKE FLOW

T. S. Mautner
Naval Command, Control & Ocean
Surveillance Center RDTE Division
San Diego, CA 92152

ABSTRACT

The sound generated by uniform flow over a heated cylinder is calculated for a range of Reynolds and Grashof numbers. The time-dependent, incompressible flow field is computed using a vorticity-stream function method containing the Boussinesq approximation. Using the computed incompressible flow field, the radiated sound is computed using a low frequency Green's function technique. Snapshots of the vorticity and temperature fields and time histories of the radiated sound pressure are presented and compared with existing results.

NOMENCLATURE

a_0	Sound speed
C_D	Drag coefficient
F_B	Buoyant force
Gr	Grashof number
Gr/Re^2	Buoyancy parameter
M_0	Mach number
Nu	Nusselt number
p	Pressure
Pr	Prandtl number
P_s	Sound pressure
r, R, R_0, R_{max}	Radius
Re	Reynolds number
St	Strouhal number
t	Time
T, T_0, T_{wall}	Temperature
U, V, V_r, V_θ	Velocity components
x	Coordinate position
y	Spatial coordinate
Y	Potential function
α	Volume Expansion
κ	Thermal conductivity
μ	Dynamic viscosity
Ω	Vorticity
ψ	Stream function
ρ, ρ_0	Density
θ	Angular coordinate
ξ, η	Transformed coordinates

INTRODUCTION

The noise radiated from the low Mach number flow around a cylinder is a fundamental acoustic process, and it is this kind of time dependent wake flow which can be found in various engineering fields, for example cooling fans. The ability to compute the sound generated by a fluid flow has been a long term goal of acoustics community. Pioneering work by Lighthill⁸ and others has led to many approaches for determining flow generated sound. A problem common to most approaches is the assumption that the source terms are either known from experiment or can be adequately modeled.

It is safe to say that the terms involved in the complete acoustic formulation, for example Lighthill's acoustic analogy, are very difficult to measure and must be simplified for either calculation or determination by experiment. An alternate approach to specification of the source terms would be computation of the flow field using the full Navier-Stokes equations. The mature field of Computational Fluid Dynamics (CFD) makes it realistic to think that numerical solutions to the Navier-Stokes equations can be obtained with sufficient accuracy to provide the inputs required by the acoustic equations. A sample of the many numerical studies of cylinder flows can be found in Refs. 2,3,7,9 and 11.

A Computational Acoustics (CA) approach has been used by several researchers to compute the sound generated by low Mach number flows about circular cylinders. It is well known that cylinders have been the object of countless experimental, numerical and analytical studies over the years. Thus the phenomena of vortex shedding is well understood and provides a suitable platform for developing techniques to compute the dipole radiation at low Reynolds numbers. Blake¹ provides an extensive review of the work associated with dipole sound radiated from cylinders while the numerical results of Hardin and Lampkin,⁴ for example, have shown good agreement in the radiated sound pressure obtained from numerical solutions and experimental data.

The above mentioned acoustic computations provide the motivation for this work. Thus, the purpose of the numerical experiments presented herein is to predict the radiated sound pressure of a heated cylinder in a uniform

This paper is declared work of the U.S. Government and is not subject to copyright protection in the United States.

flow field. Computation of the far field radiated sound is determined using a two step approach. First, the time dependent incompressible flow field is computed using CFD techniques. Second, the acoustic pressure is computed via an integral over the flow field using the low frequency Green's function pressure equation developed by Howe.^{5,6} In the following sections the CFD and CA methods will be presented along with results of the flow and sound computations.

CFD METHOD

Equations of Motion

Computational Fluid Dynamic (CFD) techniques will be used to determine the flow field data required in the acoustic calculations. The governing two dimensional equations are continuity, the Navier-Stokes equations with a buoyant force (using the Boussinesq approximation), the energy equation and an equation of state. They are

$$\nabla \cdot \vec{V} = 0 \quad (1)$$

$$\rho_0 \frac{D\vec{V}}{Dt} = \vec{F}_B - \nabla \vec{p} + \mu \nabla^2 \vec{V} \quad (2)$$

$$\frac{D\vec{T}}{Dt} = \kappa \nabla^2 \vec{T} \quad (3)$$

$$\rho = \rho_0 [1 - \alpha(T - T_0)] \quad (4)$$

Solution of the above equations, for the geometry shown in Fig. 1, makes use of a vorticity-stream function in polar coordinates. The two dimensional velocity components in terms of the stream function ψ are

$$V_r = \frac{1}{r} \frac{\partial \psi}{\partial \theta} \quad V_\theta = -\frac{\partial \psi}{\partial r} \quad (5)$$

and the vorticity is

$$\Omega = \frac{1}{r} \frac{\partial(rV_\theta)}{\partial r} - \frac{1}{r} \frac{\partial V_r}{\partial \theta} \quad (6)$$

The equations are non-dimensionalized with respect to the cylinder radius, free stream velocity and a reference temperature difference. To resolve flow gradients near the cylinder wall, the following grid stretching transformation is used

$$r = e^{\pi \xi} \quad \theta = \pi \eta \quad g = \pi^2 e^{2\pi \xi} \quad (7)$$

After applying the above definitions, the flow equations assume the form^{2,9}

$$\frac{\partial^2 \psi}{\partial \xi^2} + \frac{\partial^2 \psi}{\partial \eta^2} = -g \Omega \quad (8)$$

$$\begin{aligned} & g \frac{\partial \Omega}{\partial t} + \frac{\partial(V_r \Omega)}{\partial \xi} - \frac{\partial(V_\theta \Omega)}{\partial \eta} \\ &= \sqrt{g} \frac{Gr}{Re^2} \left\{ \sin \pi \eta \frac{\partial T}{\partial \xi} - \cos \pi \eta \frac{\partial T}{\partial \eta} \right\} \\ & \quad + \frac{2}{Re} \left[\frac{\partial^2 \Omega}{\partial \xi^2} + \frac{\partial^2 \Omega}{\partial \eta^2} \right] \end{aligned} \quad (9)$$

and

$$\begin{aligned} & g \frac{\partial T}{\partial t} + \frac{\partial(V_r T)}{\partial \xi} - \frac{\partial(V_\theta T)}{\partial \eta} \\ &= \frac{1}{Pr Re} \left[\frac{\partial^2 T}{\partial \xi^2} + \frac{\partial^2 T}{\partial \eta^2} \right] \end{aligned} \quad (10)$$

The equations are solved in the computational domain $0 \leq \xi \leq \xi_{max}$ and $0 \leq \eta \leq \eta_{max}$ with the initial conditions of $V_r = V_\theta = T = \Omega = 0$. The boundary conditions are

$$\psi = \frac{\partial \psi}{\partial \xi} = 0 \text{ on } \xi = 0 \text{ and } 0 \leq \eta \leq \eta_{max}$$

$$\psi = -2 \sinh \pi \xi \sin \pi \eta \text{ and } \Omega = 0$$

$$\text{on } \xi = \xi_{max} \text{ and } 0 \leq \eta \leq \eta_{max}$$

For cylinder heating, a uniform temperature ($T_{wall}=1.0$) is applied on the cylinder wall ($\xi=0$) after a $t=1$ startup time. Periodic boundary conditions are applied at $\eta=1$ and η_{max} for $0 \leq \xi \leq \xi_{max}$, and the vorticity Ω is extrapolated to the outflow boundary within the region $\theta_{lim} = \pm 45^\circ$.

Additionally, several flow and heat transfer quantities are evaluated. The cylinder surface pressure is computed using

$$p(\theta) = \frac{4}{Re} \int_0^\theta \Omega(\theta) \xi|_{\xi=0} d\theta + \frac{Gr}{Re^2} \sin \theta \quad (11)$$

the drag coefficient is obtained from

$$C_D = \frac{2}{Re} \int_0^{2\pi} \left[\Omega(\theta) \xi|_{\xi=0} + \Omega(\theta) \xi=0 \right] \sin \theta d\theta \quad (12)$$

while the Nusselt number and its average are obtained using

$$Nu(\theta) = -2 \left[\frac{\partial T(\theta)}{\partial \xi} \right]_{\xi=0} \quad (13)$$

and

$$Nu_{AVG} = \frac{1}{2\pi} \int_0^{2\pi} Nu(\theta) d\theta \quad (14)$$

Solution Method

The vorticity and temperature equations were solved using a method developed by Torrance and Rockett¹² with modification⁹ to the body force terms. Both equations can

be considered in the form

$$\frac{\partial P}{\partial t} = -\frac{\partial(UP)}{\partial X} - \frac{\partial(VP)}{\partial Y} + A_1 \frac{\partial Q}{\partial X} + A_2 \frac{\partial Q}{\partial Y} + B \left[\frac{\partial^2 P}{\partial X^2} + \frac{\partial^2 P}{\partial Y^2} \right] \quad (15)$$

Upwind differencing is used for the first two terms on the right hand side of the equation, central differencing for the terms multiplied by A_1, A_2 and B , and forward differencing for the time on the left hand side of Eqn. (15). Poisson's equation for the stream function is solved using a successive overrelaxation method. Details of the method are given in Ref. 9.

CA METHOD

Results of flow field calculations yield time histories of the vorticity, stream function and velocity components throughout the computational domain. These data will be used to compute the sound generated by the cylinder's wake flow.

The method used herein is that of Howe^{5,6} who considered the sound generated by a body in a non-uniform flow. The flow to be considered is isentropic and has as its only important noise source a dipole ($\text{div}(\vec{\Omega} \times \vec{V})$). The source is assumed to be compact, and the mean flow has a Mach number satisfying $M_0^2 \ll 1$ which implies that the flow is incompressible with a constant speed of sound. Howe determined that this kind of flow can be approximated by the convective wave equation, and considering the case of a turbulent eddy convected past a rigid body, Howe determined that, using his low frequency Green's function, the sound radiation has the form

$$B = -c_1 \frac{\partial}{\partial t} \int \left[\vec{\Omega} \times \vec{V} \cdot \nabla \left\{ \left[\frac{\vec{x}}{|\vec{x}|} - \vec{M}_0 \right] \cdot \vec{V} \right\} \right] d^3 y \quad (16)$$

where $c_1 = 1/(4\pi a_0 |\vec{x}|)$ and \vec{V} is the potential of the incompressible flow about the body and is of unit speed at large distances from the body. The quantity within the square brackets is evaluated at the retarded time $t - (|\vec{x}| - \vec{M}_0 \cdot \vec{x})/a_0$.

Introducing a velocity which is parallel to the normal of the wave fronts reaching the observation point \vec{x} and noting that the wavelength λ of the sound satisfies the relation $\lambda/2R = 1/StM_0$, the conditions for application of the low frequency Green's function method have been met. Thus the expression for the sound radiated to the far field observer located at \vec{x} at time t is

$$p(\vec{x}, t) = -\frac{P}{4\pi a_0 x \left[1 + \vec{M}_0 \cdot \frac{\vec{x}}{x} \right]} \frac{\partial}{\partial t} \int_{\Omega} \left[(\vec{\Omega} \times \vec{V}) \cdot \nabla \left\{ \left[\frac{\vec{x}}{x} - \vec{M}_0 \right] \cdot \vec{V} \right\} \right] dy \quad (17)$$

where $x = |\vec{x}|$, $\vec{M} = (U/a_0, 0, 0)$, $\vec{\Omega} = (0, 0, \Omega)$, $\vec{V} = (V_r, V_\theta, 0)$ and the quantity within the square brackets is evaluated at the retarded time. Noting that $r^2 = y_1^2 + y_2^2$, the potential \vec{V} is

$$\vec{V} = (\phi_1, \phi_2, y_3) = \left[y_1 \left[1 + \frac{1}{r^2} \right], y_2 \left[1 + \frac{1}{r^2} \right], y_3 \right] \quad (18)$$

Neglecting the Mach number dependence, Eqn. (17) for two dimensional flow becomes

$$p(\vec{x}, t) = \frac{\rho_0}{4\pi a_0 x^2} \frac{\partial}{\partial t} \left[x_1 \int dy_1 \int dy_2 \Omega \left[V_r \frac{\partial \phi_1}{\partial y_2} - V_\theta \frac{\partial \phi_1}{\partial y_1} \right] + x_2 \int dy_1 \int dy_2 \Omega \left[V_r \frac{\partial \phi_2}{\partial y_2} - V_\theta \frac{\partial \phi_2}{\partial y_1} \right] \right] \quad (19)$$

In transformed coordinates, the sound integral term (within the square brackets) becomes a function of (ξ, η) . If the source can be considered compact, one can neglect the variation of retarded time across the source. The sound integral was computed at each time step, and the acoustic pressure was determined by computing the time derivative of the sound integral. This was accomplished by using five point averaging on the sound integral data and 4th order central difference expressions for the time derivative. Results of the flow and acoustic computations will be presented in the next section.

RESULTS

Natural Vortex Shedding

The first case considered was the effect of grid size on natural vortex shedding at three Reynolds numbers, $Re=100, 200$, and 500 . As pointed out by Rosenfeld,¹⁰ solution convergence may not occur for cylinder grid sizes less than approximately 257×257 . However, to keep the computation times at a reasonable level, grid densities of 101×101 and 201×201 were used to demonstrate the effect of grid size on the solution.

The results are given in Figs. 2-6 for 101^2 grid and in Figs. 7-13 for the 201^2 grid. Examination of the vorticity contours shows how much flow detail is lost using the 101^2 grid. At the same time comparable results were obtained for the surface vorticity and pressure. Additionally, the com-

puted drag coefficients are given in Table 1 below and agree well with existing data, for example Son and Hanratty.¹¹ These data suggest that reasonable values of surface data and drag can be obtained using the smaller grid size.

Table 1. Computed drag coefficients for natural vortex shedding.

Re	101 ² Grid C _D	201 ² Grid C _D
100	1.095	1.156
200	0.951	1.083
500	0.823	1.027

Comparison of the computed sound integral shows substantial changes in the signatures for the two grids. The 101² grid sound data for Re=200 agrees well, at least qualitatively, with the results of Hardin⁴ et al. The significant change in sound signatures using the larger grid makes one question if the solution has converged to its final value. It should also be noted that the estimated Strouhal number for Re=200 yields St=0.17 as compared to the accepted experimental value of St=0.19–0.20. A lower value of St is found for all the data and reflects what is believed to be dissipation introduced by the numerical method in this highly convective flow. However, it is felt that the results for bulk flow properties and signature characteristics are representative of the cases considered herein. The current results and the data of Rosenfeld¹⁰ indicate the need to use the 201x201 grid for the heated cylinder computations to be presented in the following section.

Uniform Wall Temperature

Numerical experiments were conducted to examine the effects of uniform wall heating and variation of the buoyancy parameter Gr/Re^2 on the vorticity and radiated sound. The results of these calculations are presented in Figs. 14-49 and Table 2 below for Re=100, 200 and 500 and $Gr/Re^2=0-5.0$.

After a startup time of $t=1.0$, the uniform wall temperature $T=1.0$ was applied. The isotherms at $t=100$ were constructed using a range of $0.5 \leq T \leq 1.0$ to limit the contours in the high temperature gradient region near the cylinder wall. The vorticity and isotherm data show that as the buoyancy parameter is increased, the symmetrical nature of the wake is lost and large variations of vorticity and temperature are found in the upper wake region. For Re=100 and 200, the vorticity and temperature contours show elimination of the wake fluctuations when $Gr/Re^2=2.5$ and 5.0. However, the wake fluctuations of vorticity and temperature remain for all values of Gr/Re^2 for the Re=500 case. In all cases, the isotherms follow the vorticity and heating of the

fluid only occurs in the wake region of the flow. These trends have been obtained in previous numerical studies^{2,3,7}.

The distribution of surface vorticity, pressure and Nusselt number have also been presented for the various Re and Gr/Re^2 at $t=100$. These data show the increase in magnitude of vorticity, pressure and Nusselt number with increasing Re and Gr/Re^2 . The data also show the largest variation in the rear portion of the cylinder which is strongly affected by the wake conditions. The computed drag coefficients and average Nusselt numbers are given in Table 2 and show an increase with both Re and Gr/Re^2 . The Nu_{AVG} data agrees well with the extrapolated data ($t \rightarrow \infty$) of Jain and Goal⁷ for Re=100 and 200.

Table 2. Computed drag coefficients and Nusselt numbers for various Re and Gr/Re^2 .

Re	Gr/Re^2	C _D	Nu_{AVG}
100	0	1.156	---
	0.25	1.170	5.077
	0.0	1.190	5.115
	1.0	1.198	5.235
	2.5	1.349	5.561
	5.0	1.622	6.006
200	0	1.083	---
	0.25	1.095	7.355
	0.5	1.098	7.375
	1.0	1.160	7.590
	2.5	1.179	7.790
	5.0	1.549	8.313
500	0	1.027	---
	0.25	1.074	11.867
	0.5	1.034	12.228
	1.0	1.032	12.252
	2.5	1.188	12.811
	5.0	1.589	12.642

Using Eqn. (19), the time history of the radiated sound integral (proportional to the radiated sound pressure) was computed for several angular positions, ($0^\circ \leq \theta \leq 90^\circ$), for each Re and Gr/Re^2 . Examination of the data shows the periodic nature of the acoustic radiation and the increase in magnitude with increasing Reynolds number and the change in signature character for increasing Gr/Re^2 . Although not shown, the radiated sound becomes \approx zero for $Gr/Re^2=2.5$ and 5.0 for Re=100 and $Gr/Re^2=5.0$ for Re=200 which reflects the elimination of vorticity fluctuations in the heated wake. Similar results were obtained by Mautner⁹ for cylinder wake flows in stratified flow. The details of the signatures can be obtained from the figures. However, it should be noted that as the wall heating and buoyancy begin to

modify the wake vorticity, the radiated sound signatures lose the sinusoidal nature found for $T=0$ and reflect the wake fluctuations over $0 \leq \theta \leq 90^\circ$. This would suggest that not only is the magnitude of the radiated sound increased in the heated wake, but a larger spectrum of frequencies of sound, in addition to the fundamental, will be radiated into the far field.

CONCLUSIONS

The problem of laminar mixed convection from a heated cylinder has been investigated numerically by solving the Navier-Stokes and energy equations over a range of Re and Gr/Re^2 . The radiated sound has been computed using a low frequency Green's function method. The effect of grid size on solution convergence dictated the use of a 201^2 grid for the heated cylinder flow and acoustic computations. The natural shedding results were in good agreement with previous results as were the trends in the temperature contours for various values of the buoyancy parameter. The radiated sound results were in qualitative agreement with existing data for $Re=200$ using the 101^2 grid. However, low values of Strouhal number indicate excessive dissipation introduced by the numerical method. The acoustic results show significant changes in the signature shape with increasing Gr/Re^2 and magnitude increases with increasing Re . The computed values of drag coefficient, surface pressure, vorticity and Nusselt number agree well with existing data. Even though the small grid size, (101^2), allows for reasonable values of bulk parameters, for example drag, higher density grids are required to obtain solution convergence. The change in character of the radiated sound from the 101^2 grid to the 201^2 grid suggests that a finer grid may be required to obtain solution convergence. Finally, the nature of the radiated sound in the heated wake suggests that a much broader range of frequencies will be present in the far field sound.

ACKNOWLEDGMENT

This work was sponsored by this Division's High Performance Computing Fellowship Program. Cray YMP time was provided by the DoD High Performance Computing Center, USAR Waterways Experiment Station, Vicksburg, MS.

REFERENCES

1. Blake, W. K., *Mechanics of Flow-Induced Sound and Vibration*, Vol. 1, Academic Press, Inc., Orlando, 1986.
2. Badd, H. M., A Theoretical Study of Laminar Mixed Convection from a Horizontal Cylinder in a Cross Stream, *Int. J. Heat & Mass Transfer*, Vol. 26, 1983, p. 639.

3. Chen, C-H. and Weng, F-B., Heat Transfer for Incompressible and Compressible Fluid Flows over a Heated Cylinder, *Numerical Heat Transfer*, Vol. 18, 1990, p. 325.
4. Hardin, J. C. and Lamkin, S. L., Aeroacoustic Computation of Cylinder Wake Flow, *AIAA Journal*, Vol. 22, No. 1, 1984, p.51.
5. Howe, M. S., The Generation of Sound by Aerodynamic Sources in an Inhomogeneous Steady Flow. *J. Fluid Mech.*, Vol 67, 1975, p. 597.
6. Howe, M. S., The Theory of Aerodynamic Sound, *J. Fluid Mech.*, Vol. 71, 1975, p. 625.
7. Jain, P. C. and Goal, B. S., A Numerical Study of Unsteady Laminar Forced Convection from a Circular Cylinder, *J. Heat Transfer*, Vol. 98, 1976, p. 303.
8. Lighthill, M. J., On Sound Generated Aerodynamically, 1. General Theory, *Proc. Royal Soc., Series A*, Vol. 211, 1952, p. 564.
9. Mautner, T. S., Acoustic Computations for a Moving Cylinder in Flows with Temperature Gradients, Paper AIAA-93-2204, AIAA/ASME/SAE/ASEE 29th Joint Propulsion Conference, Monterey, CA, June, 1993.
10. Rosenfeld, M., Grid Refinement Study of Time Periodic Flow over a Circular Cylinder, Paper AIAA 93-0433, 31st Aerospace Sciences Meeting, Reno, NV, 1993.
11. Son, J. S. and Hanratty, T. J., Numerical Solution for the Flow Around a Cylinder at Reynolds Numbers of 40, 200, 500, *J. Fluid Mech.*, Vol. 35, 1969, p. 369.
12. Torrance, K. E. and Rockett, J. A., Numerical Study of Natural Convection in an Enclosure With Localized Heating From Below - Creeping flow to the Onset of Laminar Instability, *J. Fluid Mech.*, Vol. 36, 1969, p 33.

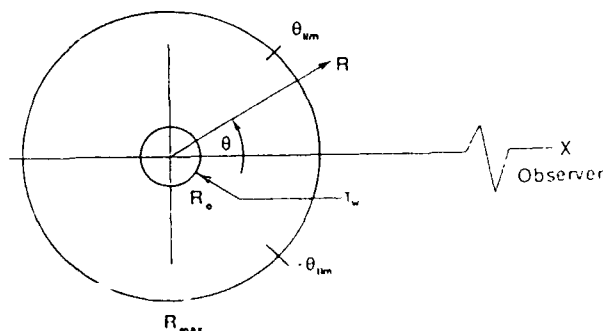


Fig. 1. Geometry

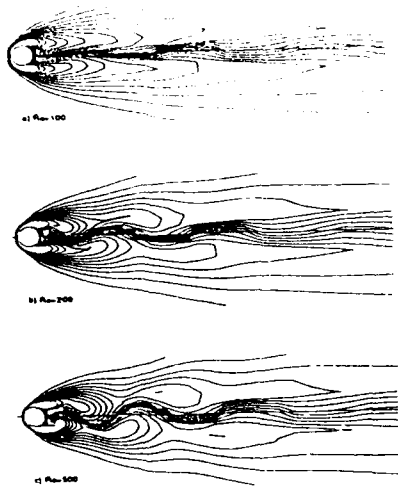


Fig. 2. Vorticity contours for 101x101 grid.

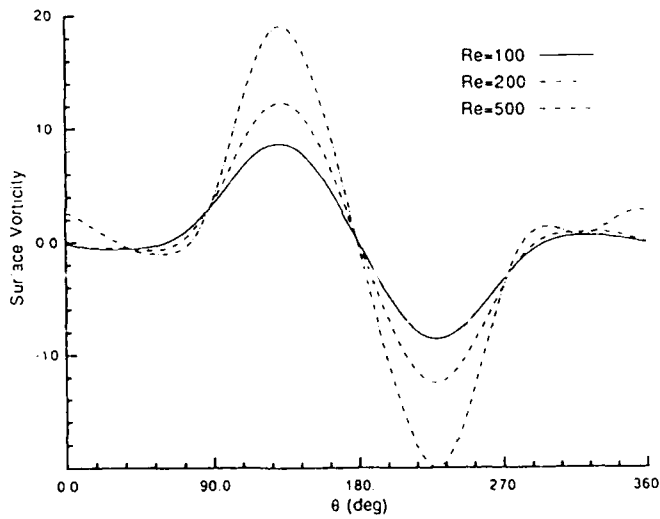


Fig. 3. Cylinder surface vorticity distributions for the 101x101 grid.

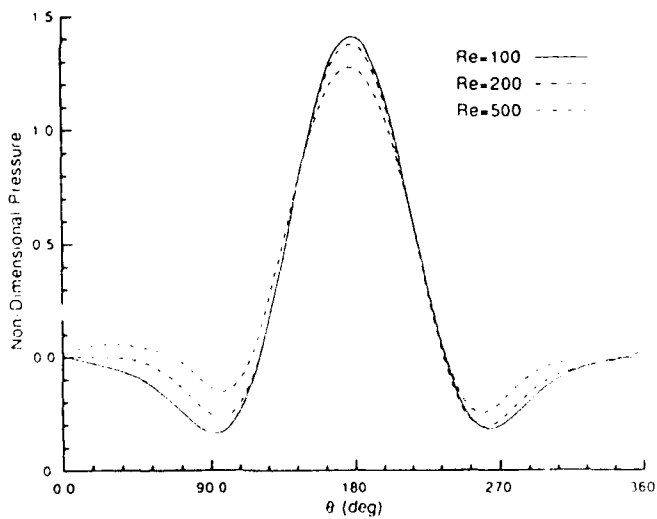


Fig. 4. Cylinder surface pressure distributions for the 101x101 grid.

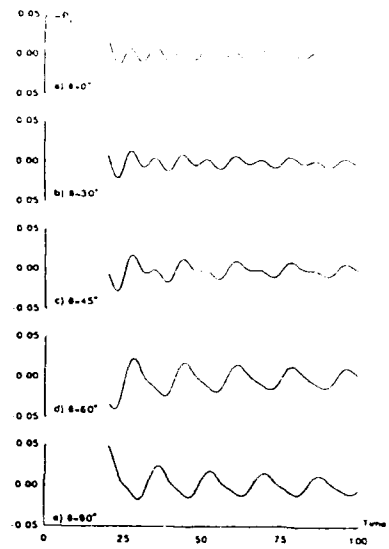


Fig. 5. Time history of the sound integral for the 101x101 grid and $Re=100$.

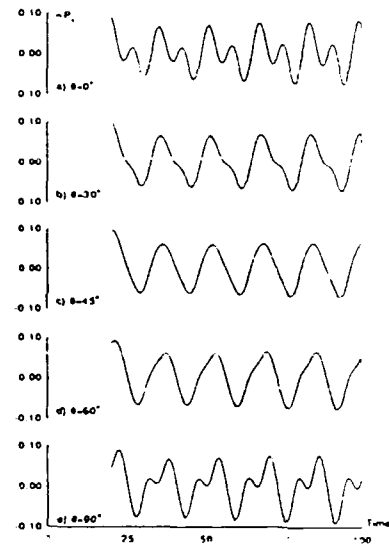


Fig. 6. Time history of the sound integral for the 101x101 grid and $Re=200$.

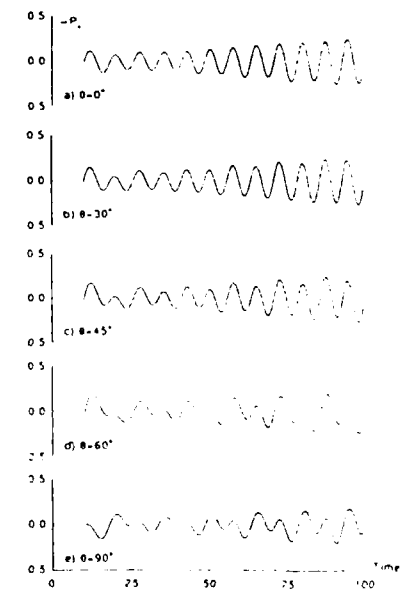


Fig. 7. Time history of the sound integral for the 101x101 grid and $Re=500$.

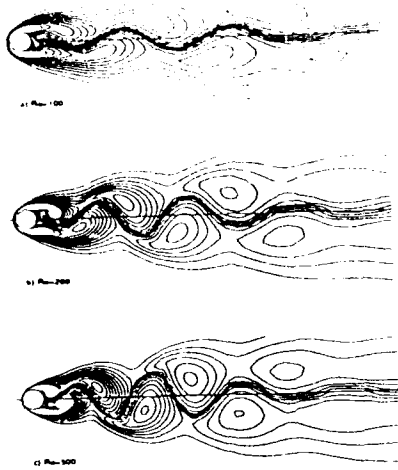


Fig. 8. Vorticity contours for 201x201 grid.

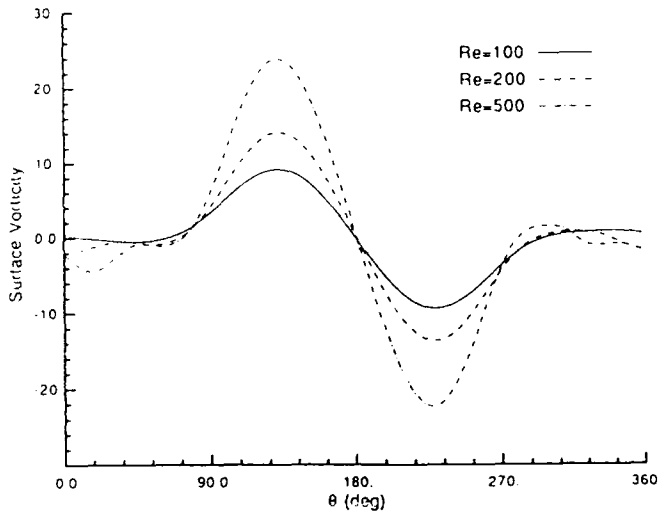


Fig. 9. Cylinder surface vorticity distributions for the 201x201 grid.

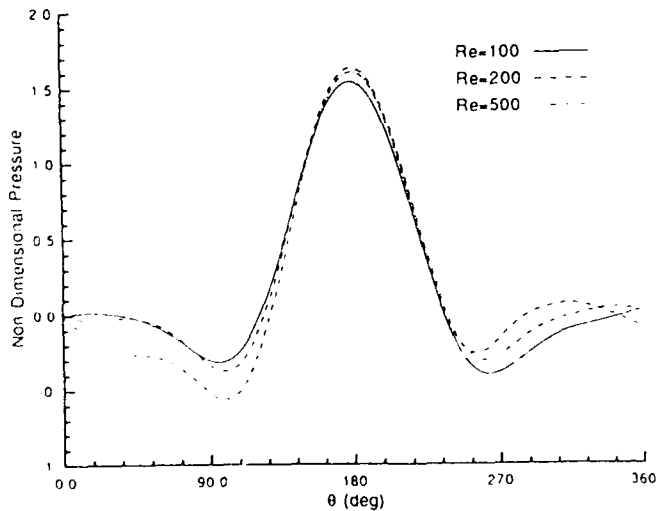


Fig. 10. Cylinder surface pressure distributions for the 201x201 grid.

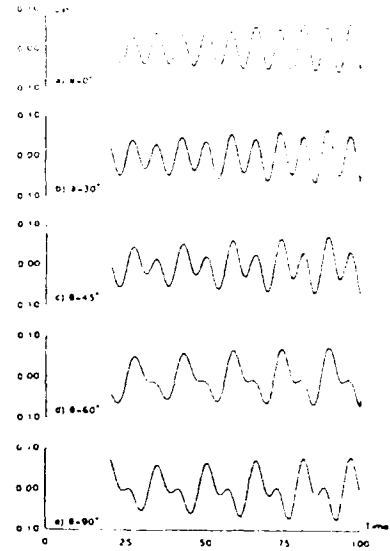


Fig. 11. Time history of the sound integral for the 201x201 grid and $Re=100$.

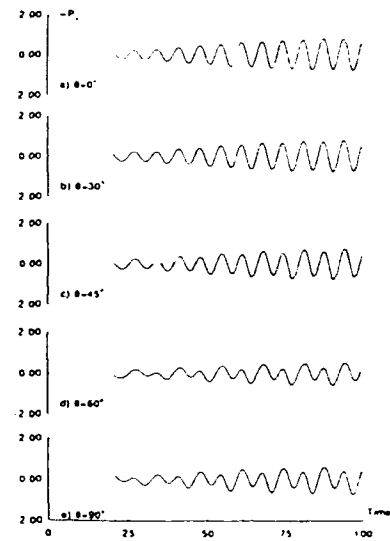


Fig. 12. Time history of the sound integral for the 201x201 grid and $Re=200$.

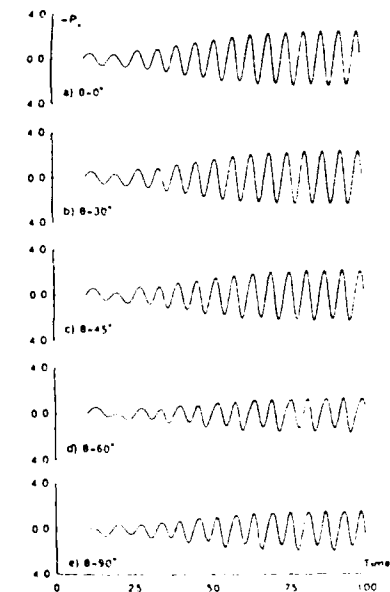


Fig. 13. Time history of the sound integral for the 201x201 grid and $Re=500$.

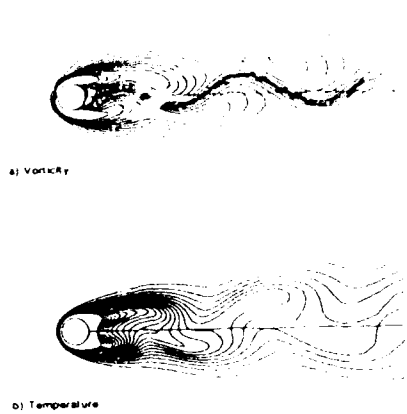


Fig. 14. Vorticity contours and isotherms for $Re=100$ and $Gr/Re^2=0.25$.

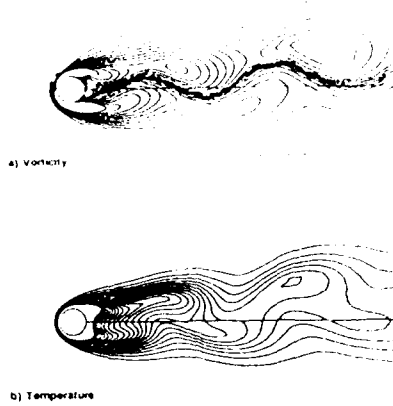


Fig. 15. Vorticity contours and isotherms for $Re=100$ and $Gr/Re^2=0.5$.

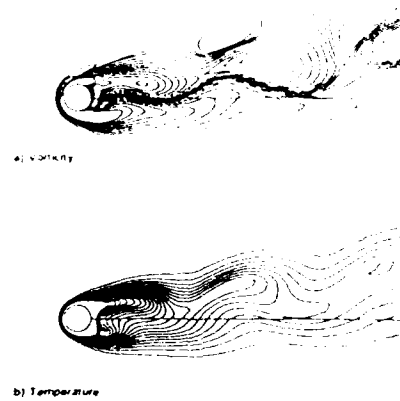


Fig. 16. Vorticity contours and isotherms for $Re=100$ and $Gr/Re^2=1.0$.

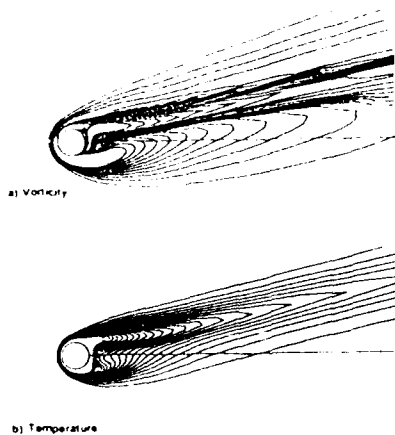


Fig. 17. Vorticity contours and isotherms for $Re=100$ and $Gr/Re^2=2.5$.

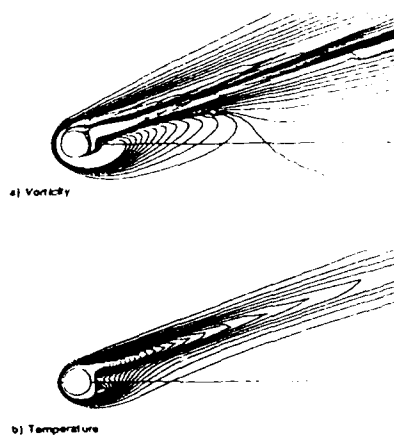


Fig. 18. Vorticity contours and isotherms for $Re=100$ and $Gr/Re^2=5.0$.

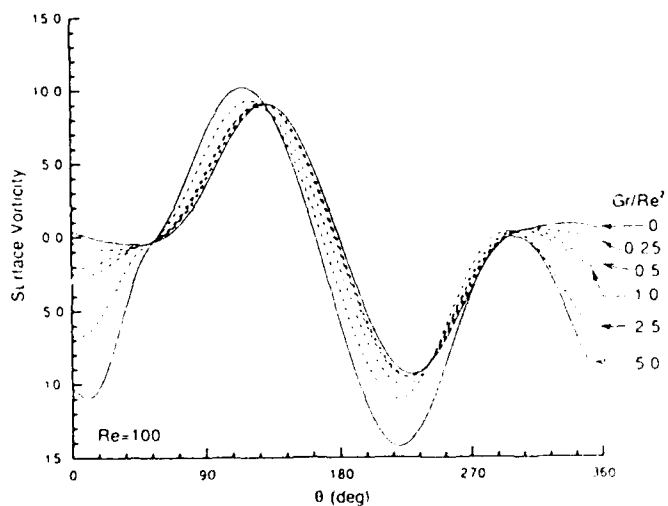


Fig. 19. Cylinder surface vorticity for $Re=100$ and $Gr/Re^2=0-5.0$.

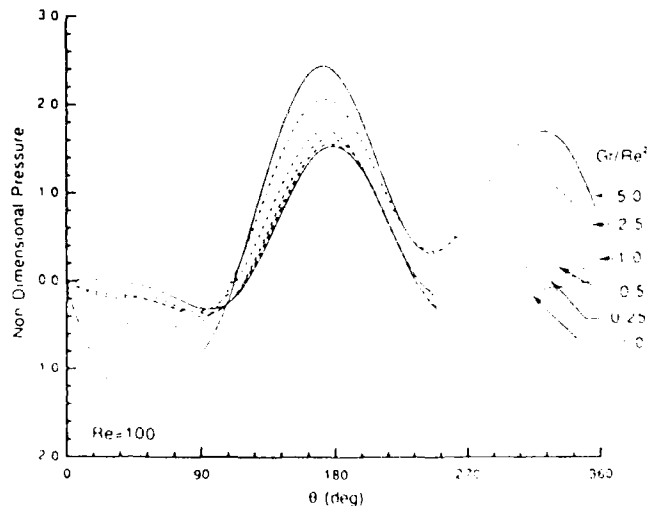


Fig. 20. Cylinder surface pressure for $Re=100$ and $Gr/Re^2=0-5.0$.

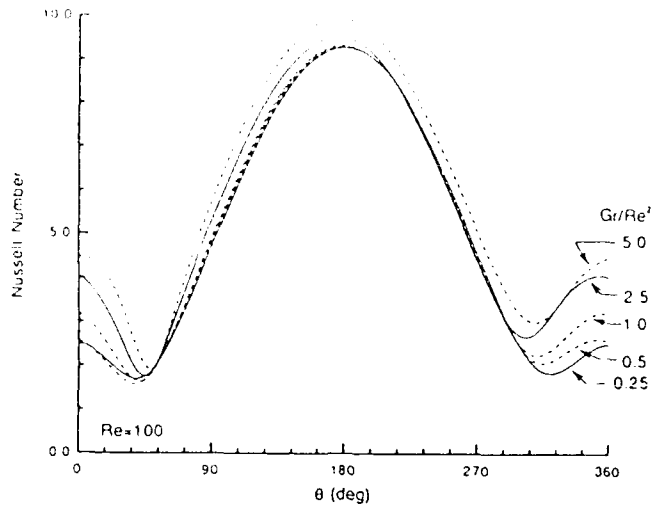


Fig. 21. Cylinder surface Nusselt number for $Re=100$ and $Gr/Re^2=0.25-5.0$.

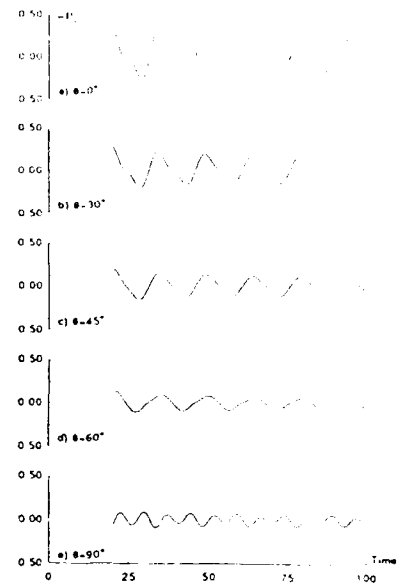


Fig. 22. Time history of the sound integral for $Re=100$ and $Gr/Re^2=0.25$.

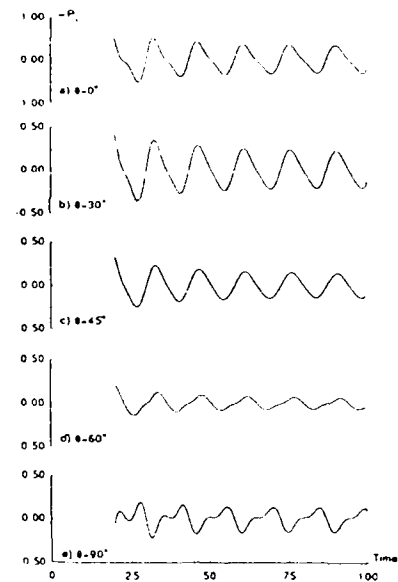


Fig. 23. Time history of the sound integral for $Re=100$ and $Gr/Re^2=0.5$.

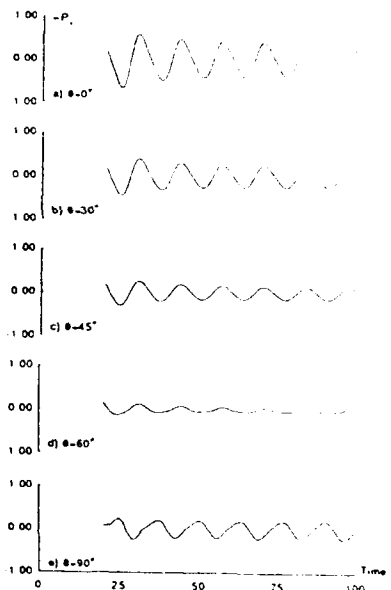


Fig. 24. Time history of the sound integral for $Re=100$ and $Gr/Re^2=1.0$.

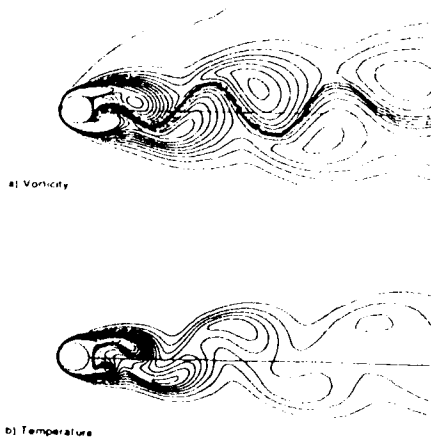


Fig. 25. Vorticity contours and isotherms for $Re=200$ and $Gr/Re^2=0.25$.

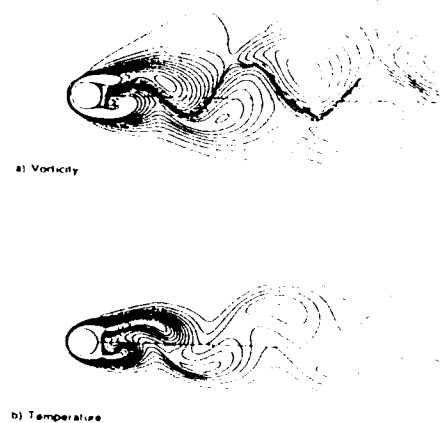


Fig. 26. Vorticity contours and isotherms for $Re=200$ and $Gr/Re^2=0.5$.

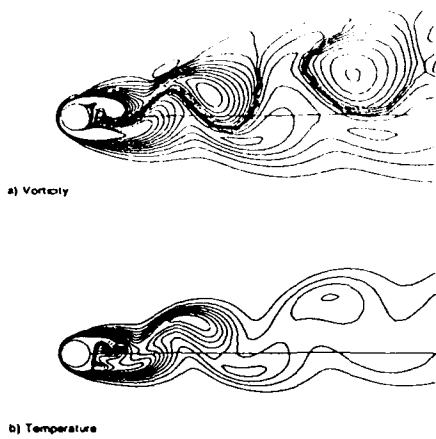


Fig. 27. Vorticity contours and isotherms for $Re=200$ and $Gr/Re^2=1.0$.

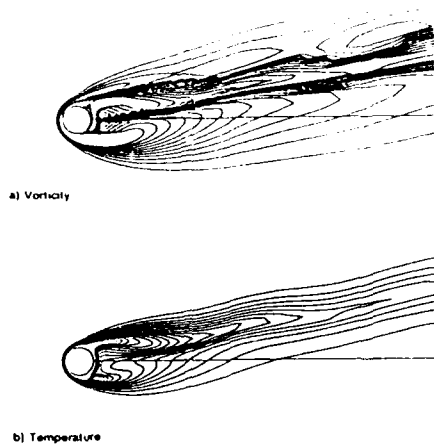


Fig. 28. Vorticity contours and isotherms for $Re=200$ and $Gr/Re^2=2.5$.

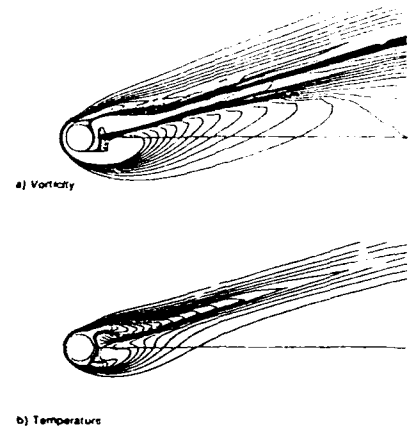


Fig. 29. Vorticity contours and isotherms for $Re=200$ and $Gr/Re^2=5.0$.

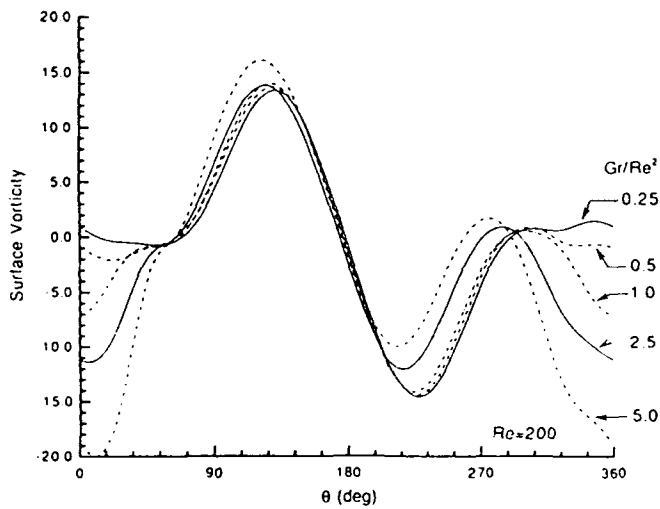


Fig. 30. Cylinder surface vorticity for $Re=200$ and $Gr/Re^2=0-5.0$.

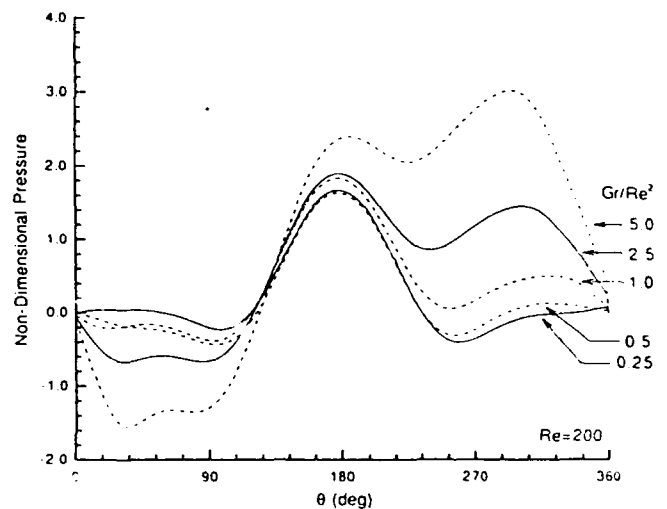


Fig. 31. Cylinder surface pressure for $Re=200$ and $Gr/Re^2=0-5.0$.

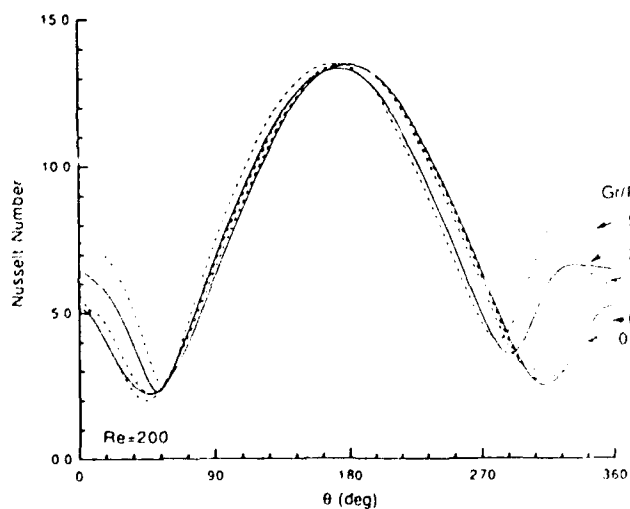


Fig. 32. Cylinder surface Nusselt number for $Re=200$ and $Gr/Re^2=0.25-5.0$.

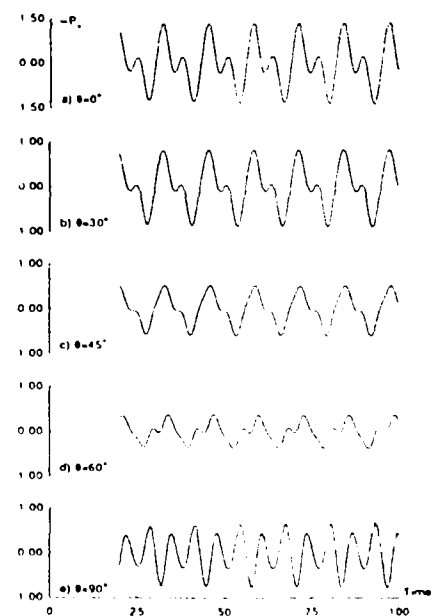


Fig. 33. Time history of the sound integral for $Re=200$ and $Gr/Re^2=0.25$.

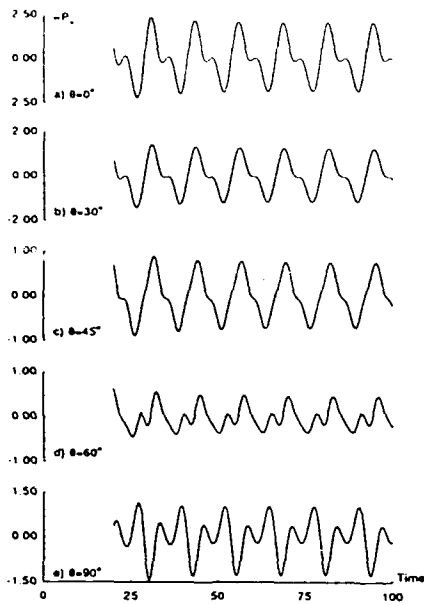


Fig. 34. Time history of the sound integral for $Re=200$ and $Gr/Re^2=0.5$.

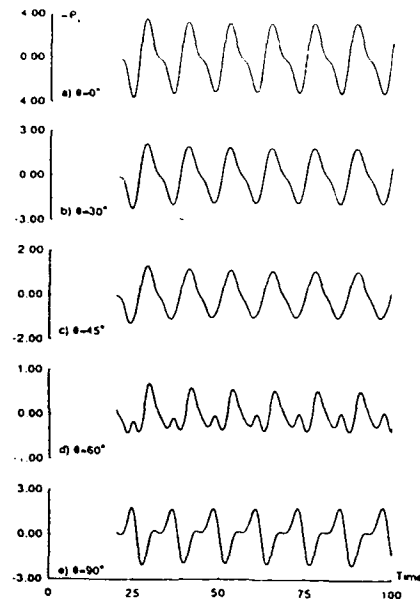


Fig. 35. Time history of the sound integral for $Re=200$ and $Gr/Re^2=1.0$.

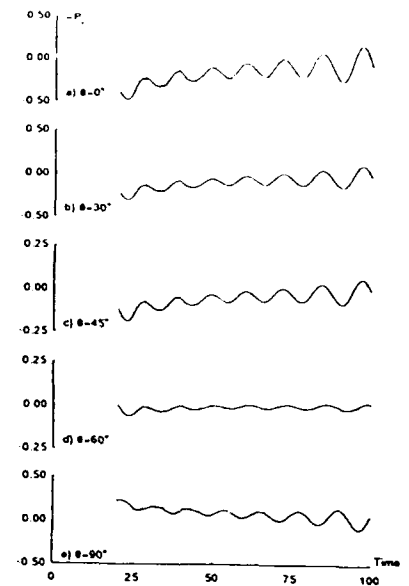


Fig. 36. Time history of the sound integral for $Re=200$ and $Gr/Re^2=2.5$.

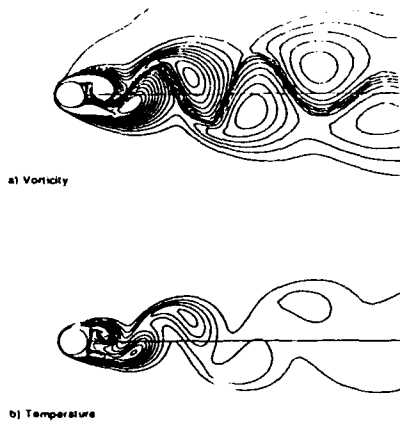


Fig. 37. Vorticity contours and isotherms for $Re=500$ and $Gr/Re^2=0.25$.

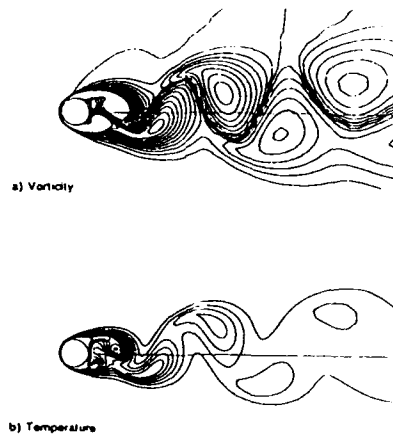


Fig. 38. Vorticity contours and isotherms for $Re=500$ and $Gr/Re^2=0.5$.

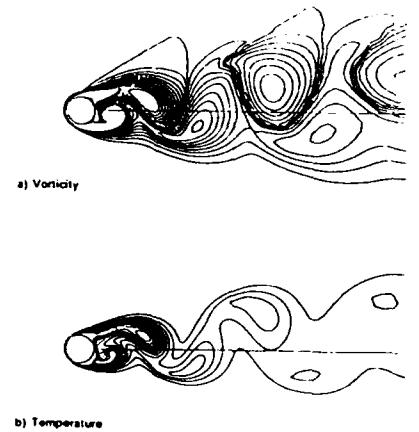


Fig. 39. Vorticity contours and isotherms for $Re=500$ and $Gr/Re^2=1.0$.

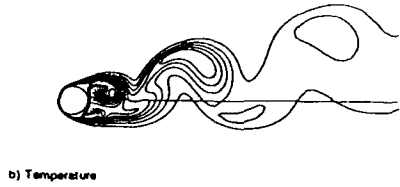
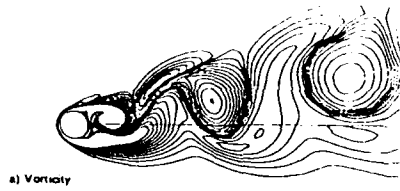


Fig. 40. Vorticity contours and isotherms for $Re=500$ and $Gr/Re^2=2.5$.

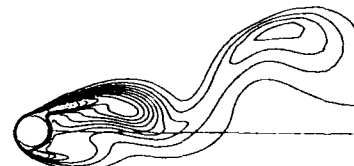
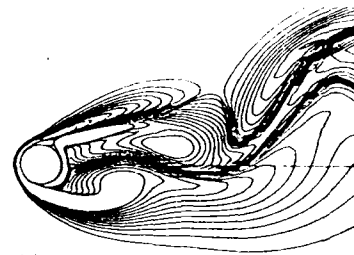


Fig. 41. Vorticity contours and isotherms for $Re=500$ and $Gr/Re^2=5.0$.

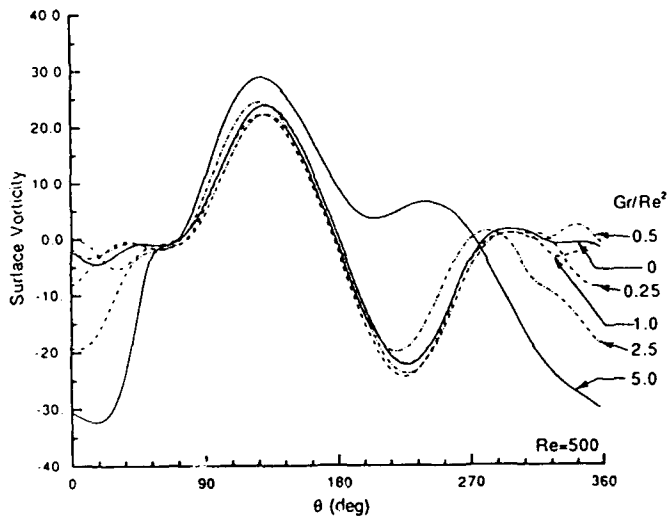


Fig. 42. Cylinder surface vorticity for $Re=500$ and $Gr/Re^2=0-5.0$.

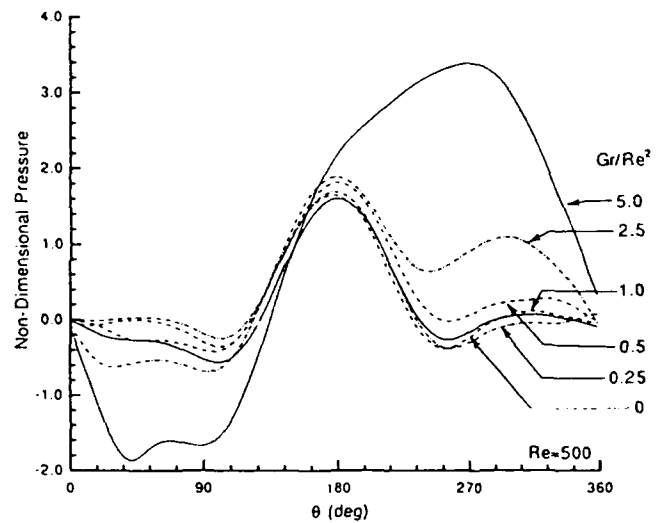


Fig. 43. Cylinder surface pressure for $Re=500$ and $Gr/Re^2=0-5.0$.

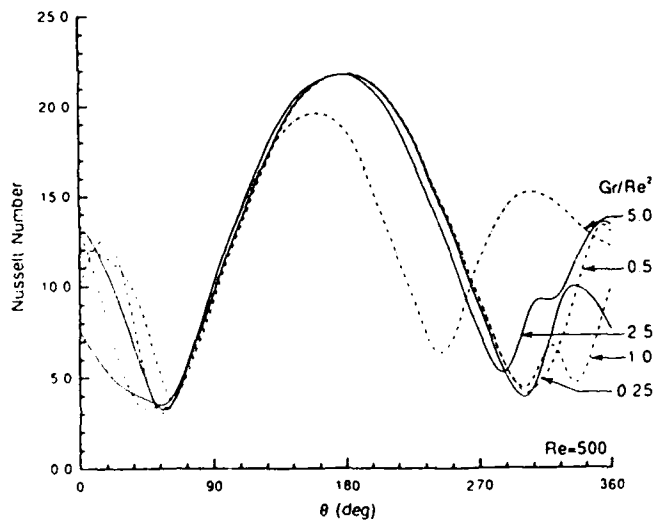


Fig. 44. Cylinder surface Nusselt number for $Re=500$ and $Gr/Re^2=0.25-5.0$.

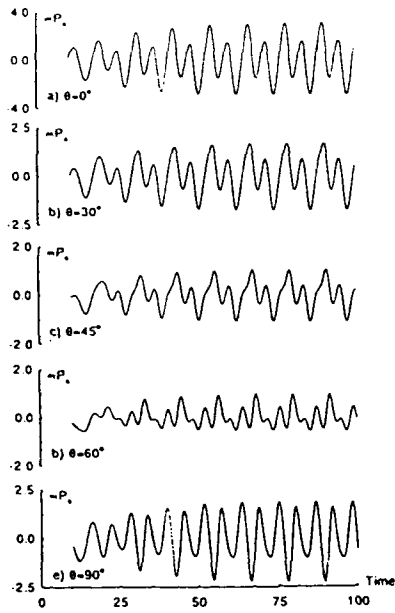


Fig. 45. Time history of the sound integral for $Re=500$ and $Gr/Re^2=0.25$.

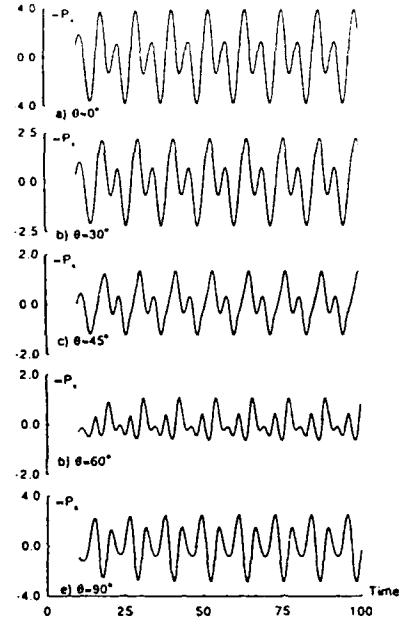


Fig. 46. Time history of the sound integral for $Re=500$ and $Gr/Re^2=0.5$.

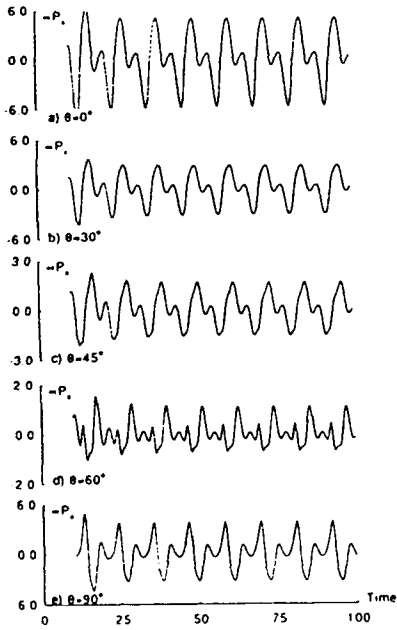


Fig. 47. Time history of the sound integral for $Re=500$ and $Gr/Re^2=1.0$.

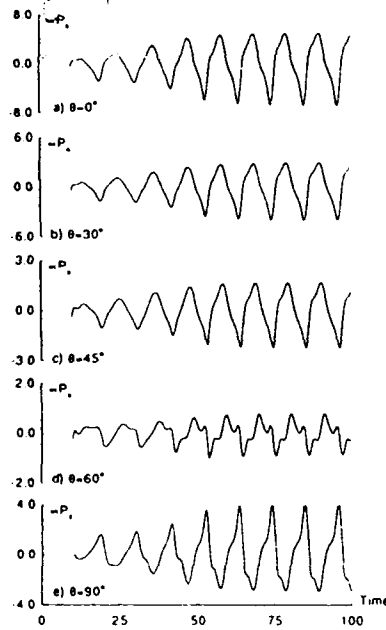


Fig. 48. Time history of the sound integral for $Re=500$ and $Gr/Re^2=2.5$.

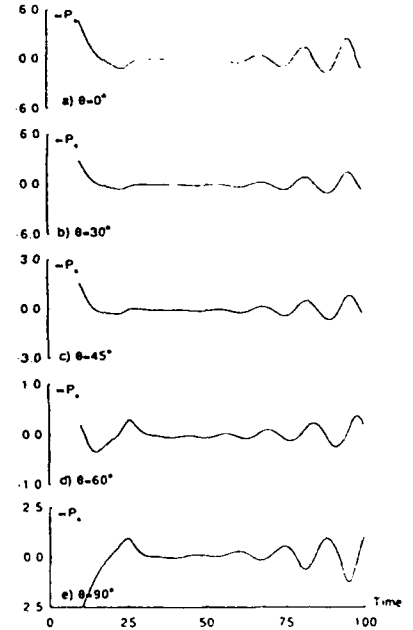


Fig. 49. Time history of the sound integral for $Re=500$ and $Gr/Re^2=5.0$.